Research Square

Preprints are preliminary reports that have not undergone peer review.
They should not be considered conclusive, used to inform clinical practice,
or referenced by the media as validated information.

Cr-doped mesoporous M1 phase MoVTeNbOx catalyze selective oxidation of propane to acrylic acid

Haonan Qu
Shenyang University of Chemical Technology
Shuangming Li
Shenyang University of Chemical Technology
Yiwen Wang
Shenyang University of Chemical Technology
Jiao Song
Shenyang University of Chemical Technology
Zhe Li
China Kunlun Contracting & Engingeering Corporation Shenyang Company
Sansan Yu (ssyu@syuct.edu.cn)
Shenyang University of Chemical Technology
Yitong Zhou
Shenyang University of Chemical Technology
Ruiqi Zhu
Shenyang University of Chemical Technology

Research Article

Keywords: MoVTeNbOx, Spray drying, Cr doping, Mesoporous, Selective oxidation of propane

Posted Date: December 21st, 2023

DOI: https://doi.org/10.21203/rs.3.rs-3728450/v1

License: This work is licensed under a Creative Commons Attribution 4.0 International License.
Read Full License

Additional Declarations: No competing interests reported.

Version of Record: A version of this preprint was published at Catalysis Surveys from Asia on February 5th, 2024. See the published version at https://doi.org/10.1007/s10563-024-09422-5.

Abstract

In this work, we investigated the doping of $MoVTeNbO_x$ catalysts with a small amount of Cr using spray drying. The effect of Cr doping on their crystalline phase structure, physicochemical properties, and catalytic propane oxidation to acrylic acid performance was investigated. The results showed that the catalyst samples were prepared by spray drying from rod stacking into unique spherical shapes. In addition, Cr doping induced a change in the mesopore structure formed by rod stacking, reducing the pore radius of the catalysts from 5–10 nm to 2–4 nm. Meanwhile, Cr doping dramatically reduced the average particle size of the motivations, decreasing the rod cross-sectional area of the catalysts from 234.21 nm to 134.96 nm and the rod length from 1.096 μm to 485.71 nm, which significantly increased the number of (001) active crystalline surfaces. Not only that, Cr doping increased the V^{5+} content on the catalyst surface from 35.8–72.6%. Together with the mesoporous structure, the Cr-doped $MoVTeNbO_x$ showed excellent performance in catalyzing the propane-selective acrylic acid production reaction. Among them, the S-3 sample (V: Cr = 1:0.015) increased the selectivity of acrylic acid from 67.5–84.3% and the acrylic acid yield from 26.4–43.2% when the reaction temperature was 380°C.

1. Introduction

Acrylic acid (AA) is an important organic chemical raw material and a common intermediate[1]. The unsaturated double bond and carboxylic acid structure of acrylic acid give it suitable polymerization and esterification functions, and it can be derived from various acrylate compounds. These compounds are widely used in coatings, adhesives, chemical fibers, textiles, hygiene products[2], etc. In recent years, the global demand for acrylic acid has been increasing year by year. With the continuous development and application of acrylic acid downstream products, acrylic acid also shows unprecedented market prospects.

Currently, more studies are conducted to generate acrylic acid by catalyzing the selective oxidation of propane/propylene. Among them, $MoVTeNbO_x$ is the most promising catalyst. $MoVNbTeO_x$ catalysts usually consist of M1 and M2 crystalline phases and a small number of other phases, such as Mo_5O_{14} structure, MoV, and MoTe oxides. The excellent catalytic activity of the M1 phase has been reliably demonstrated (the phase has an orthorhombic lattice and belongs to the Pba2 space group with lattice parameters a = 21.133 Å, b = 26.644 Å, c = 4.014 Å [3]). The M1 phase consists of centrally occupied pentagonal rings connected by MO_6 octahedra (M = Mo, V) with shared corners, which are assembled in the (001) plane to form characteristic hexagonal and heptahedral rings with TeO units, where the (001) plane is perpendicular to the length axis of the needle. It has been recognized that the M1 phase is the main active crystalline phase in alkane oxidative dehydrogenation reactions[4].

However, the high oxidizing ability of $MoVTeNbO_x$ would lead to the deep oxidation of target product acrylic acid and reduce its selectivity. Furthermore, the research on the catalysts' scale-up production and industrial application is still at a standstill. To address these issues, researchers have carried out a lot of

research work on the preparation method[5–10], doping modification[3, 11–14], loading[15, 16], and morphology modulation[4, 17]of $MoVTeNbO_x$.

Currently, the primary methods reported for the preparation of $MoVTeNbO_x$ are hydrothermal synthesis[10, 16, 18], slurry method[6, 19–21], and co-precipitation method[5, 22], but they suffer from the problems of long time-consuming, poor reproducibility of catalysts, and high requirements of preparation conditions. Spray drying[7]is a technique for rapidly converting a sprayed slurry into a dry powder by solvent evaporation, producing highly dispersed, uniformly sized solid particles in a short period. To date, various metal oxide-based samples have been prepared spray drying method[23–25]. In addition, the literature reported that $MoVTeNbO_x$ was successfully prepared by spray drying. Its catalytic activity in propane oxidation reaction was investigated[26, 27], and it was concluded that this method resulted in a more homogeneous and dispersed distribution of catalyst particles.

In addition to the preparation methods, doping hetero-atoms (K, Bi, Ca, Zr, Ga, Se, Mn, and P, etc.) in the M1 phase has also been proved to be an effective way to modulate and enhance the performance of catalysts[7, 10–12, 18, 28–30]. It is demonstrated that the introduction of Ce, and Mn can change the surface acidity and surface composition of the M1 phase, which increases the activity of the catalyst. The addition of Bi, K can replace the metal in the polygonal lattice and the atoms in the structural channels to change the superficial V^{5+}/V^{4+} ratio of the M1 phase, whereas the addition of Zr and Ca forms separate oxides that cover the active centers on the surface of the catalysts and reduce the alkane conversion. Not only that, Ishchenko et al.[31]successfully doped K and Bi into the M1-phase structure of $MoVTeNbO_x$ using spray-drying method, greatly increasing the proportion of V^{5+} in $MoVTeNbO_x$ up to 50%, which in turn improved the conversion of ethane. Kardash et al.[3]doped Se into $MoVTeNbO_x$ by spray drying and obtained highly dispersed and crystalline catalysts, but the content of V^{5+} was only increased to 45%. Among the many dopant atoms, Cr can exist in multiple valence states on the catalyst surface. These variable valence ions formed on the surface of the composite metal oxides can significantly improve the redox capacity of the catalyst, enhance the migration of the catalyst lattice oxygen, and facilitate the oxidative dehydrogenation of propane. At the same time, they may play an essential role in combination with V.

It is well known that the selective oxidation of propane to acrylic acid belongs to the gas-solid non-homogeneous reaction system, and there is reaction resistance when the gas passes through the catalyst during the reaction. Studies have shown[21, 32–37]that different pore structures and pore sizes significantly affect the adsorption capacity of the active center of the catalyst and the interaction between the motivation and the reactants and products[38].

In this work, the effect of Cr doping on the structure of M1 phase and the catalytic performance of $MoVTeNbCrO_x$ in the reaction of selective oxidation of propane to acrylic acid (AA) were investigated by spray-drying. The conformational relationship between the system and catalytic performance of

$MoVTeNbCrO_x$ were elucidated by varying the content of doped Cr, and determining the crystalline phase structure of the catalyst samples before and after doping.

2. Experimental

2.1 Catalyst preparation

The $MoVTeNbCrO_x$ (Mo:V:Te:Nb = 1:0.23:0.24:0.12)catalyst was prepared by spray drying. The initial MoVTe solution was prepared by mixing ammonium molybdate tetrahydrate, ammonium metavanadate, and telluric acid at 80°C. The prepared hydrated niobium oxalate solution and chromium nitrate solution were added into the MoVTe solution drop by drop and mixed and stirred at 80°C for 15 min to obtain a homogeneous precursor solution. The catalyst precursor was obtained by spray drying the suspension in a spray dryer (HF-015, Shanghai Hefan Instrument Co. Ltd.) at an inlet temperature of 220°C and an outlet temperature of 125°C, and was subsequently heat-treated in a nitrogen stream at 600°C. The obtained samples were stirred with 30% H_2O_2 solution at 40°C for 6 h. The pure M1 phase catalyst was obtained by filtration, washing, and drying overnight. According to the Cr doping ratio (V: Cr = 1: X, X = 0, 0.011, 0.013, 0.015, 0.017, 0.019), the prepared catalysts were named S-0, S-1, S-2, S-3, S-4, S-5, respectively.

2.2 Catalyst Characterization

The powder X-ray diffraction (XRD) patterns were recorded on an Empyrean X-ray generator (Bruker AXS Company, Germany). Scans were recorded for 2θ ° ranging from 5 to 60 ° with a step size of 0.02 ° and angle sweep rate of 5 °·min^{-1} using Cu Kα radiation. Qualitative analyses of phases were carried out by comparing the measured spectra with ICSD and Inorganics database. The morphologies and microstructures were observed by scanning electron microscope (SEM, Gemini 300-71-31) and transmission electron microscope (TEM, JEM-2100 PLUS). UV-vis measurements were performed on an UV spectrophotometer (UV-2550, Japan). The X-ray photoelectron spectroscopy (XPS) was carried out on a VG ESCALAB250 spectrometer (Thermo Fisher Scientific, USA), using a monochromatic Al (Kα) X-ray source. All binding energies (BE) were calibrated by using C1s peak of contaminant carbon (BE = 284.6 eV) as an internal standard. B250 Xi, Thermo Scientific) was used to analyze the sample surface. The specific surface areas of the samples were measured by the BET method using nitrogen adsorption-desorption isotherms by an Autosorb-IQ gas adsorption analyzer (Beijing Builder, China).

2.3 Catalytic test

The catalytic performance test of as prepared $MoVTeNbO_x$ was carried out under atmospheric pressure in a miniature fixed-bed tubular reactor (i.d. 8 mm, length 400 mm). 0.75 g of catalyst was diluted with quartz sands of the same quality, and then introduced in the middle of the reactor. Afterward, the reactor was heated to 340–420°C under the reaction gas feed flow composed of C_3H_8, H_2O, N_2 and O_2 in the mole ratio of 1.0: 2.0: 4.0: 6.2, in which the flow rate of propane was 2 mL·min^{-1}. The reaction products were collected and analyzed by a gas chromatograph (GC) equipped with a thermal conductivity detector

(TCD). CO_2, C_3H_8 and the condensate products were separated by Porapak-Q column, while O_2, N_2 and CO was separated by 13X molecular sieve column. Propane conversion (X), yield (Y) and selectivity (S) of reaction products (acrylic acid, acetic acid and carbon oxides) were defined as Eqs. (1), (2) and (3), respectively.

$$X = 1 - \frac{3f_{C_3H_8}}{3fC_3H_8 + 3f_{AA} + 2f_{C_2H_4O_2} + f_{CO} + f_{CO_2}} \times 100\% \, (1)$$

$$S = \frac{3f_{AA}}{3f_{AA} + 2f_{C_2H_4O_2} + f_{CO} + f_{CO_2}} \times 100\% \, (2)$$

$$\mathrm{Y} = \frac{S_{AA}}{X_{C_3H_8}} \times 100\% \, (3)$$

Where, $\backslash \mathrm{varvec} f$ was the molar mass of each substance.

3. Results and discussion

3.1 Structural characterization of catalysts

Figure 1a shows the crystal structures of $MoVTeNbO_x$ and $MoVTeNbCrO_x$ catalysts. These diffraction peaks located at 2θ °= 22.1, 28.24, and 45.07 ° perfectly agrees with the M1 phase (TCSD 55097)[18]. It is obvious that the doping of Cr did not change the original structure of the $MoVTeNbO_x$, and no prominent CrO_x diffraction peaks were detected. The characteristic peaks of the M1 phase at 6.59, 7.80, 8.98, and 27.13 ° are shifted after doping (Figs. 1b, c), and the more minor shifts of the S-1 and S-2 samples may be due to the small amount of doping, which does not have a substantial effect on the catalyst. The increase may be due to the replacement of Te atoms by Cr, and the atomic radius of Cr is more significant than that of the replaced Te atoms, which may be strong evidence of Cr doping in the catalyst. In addition, after washing by H_2O_2, the original M2 phase was dissolved away, leaving the crystal structure of the pure M1 phase (Fig. 1d).

The lattice parameters and cytosolic volumes calculated from the specific surface area determined by N_2 adsorption-desorption and the XRD patterns before and after Cr doping using the Rietveld method are shown in Table. 1. The results show that the specific surface area of the catalyst increases and then decreases with the gradual increase in the number of doped chromium atoms. The lattice parameter and the cytosolic volume tended to increase. The atomic radius of Cr atoms is more significant than that of Te, and the vacancies created by the loss of Te atoms are filled by Cr atoms, which may be responsible for the increase in lattice parameter and cytosolic volume, in agreement with the results of XRD analysis. Once again, it is demonstrated that Cr is successfully incorporated into the structure of $MoVTeNbO_x$.

Table 1
Physicochemical properties of $MoVTeNbO_x$ (S-0) and $MoVTeNbCrO_x$ catalyst samples doped with different percentages of $MoVTeNbCrO_x$ catalysts

Catalyst	Specific surface area (m^2/g) [a]	Lattice parameter (Å) [b]			Cytosol volume ($Å^3$) [b]
		a	b	c	
S-0	6.470	21.133	26.644	4.014	2260
S-1	8.257	21.159	26.675	4.017	2267
S-2	10.029	21.174	26.701	4.023	2274
S-3	13.688	21.198	26.723	4.019	2276
S-4	8.507	21.202	26.741	4.021	2279
S-5	7.350	21.227	26.749	4.024	2284

a

Specific surface area was measured using N_2 adsorption at liquid nitrogen temperature.

b: Simulation refinement of the cell parameters of M1 using GSAS software according to the Rietveld approach.

The SEM and TEM images of the undoped Cr catalyst are shown in Fig. 2. It can be observed from Fig. 2a and b that the catalyst samples before doping have prominent rod-like structure, which is the characteristic morphology of $MoVTeNbO_x$ catalysts. However, unlike other reports[9, 18, 21, 22, 33, 39], the catalysts prepared by the spray-drying method exhibited a morphological structure from rod-like stacking to spherical shape. This may be due to the rapid removal of solvent from the surface of the droplets during the spray drying process, which leads to a rapid increase in the solute concentration on the surface of the droplets, creating a concentration gradient. Thereby, the solute molecules in the surface region diffuse towards the center of the droplet, and thus, the solutes gradually aggregate and form spheres. The TEM and HR-TEM images of the catalyst are shown in Fig. 2c and d. It is known that the M1 phase consists of $(Te_2O)M_{20}O_{57}$ (M = Mo, V, Nb), which mainly affects the catalytic activity and selectivity of the catalyst[40–42]. From the image analysis of the S-0 catalyst, it was found (Fig. 2c) that the catalyst grows along the (001) direction to form a uniform rod-like crystal morphology eventually, and the lattice spacing of the catalyst's (001) crystalline surface can be observed to be d = 0.40 nm in Fig. 2d. In addition, EDS elemental mapping analyses of the S-0 samples showed (Figs. 2e-i) that all the elements were uniformly distributed in the catalyst.

The SEM and TEM images of the catalyst after doping with Cr are shown in Fig. 3, and after comparing Fig. 3a, b with Fig. 2a, b, it can be found that the spherical aggregation of the catalyst is complete by doping with Cr. This may be because the doping of Cr increases the concentration of the precursor liquid

per unit volume. The concentration gradient between the surface and the center of the droplet is lower when sprayed at high temperatures, and the solutes are dispersed relatively uniformly within the droplet. In this case, smoother and regular spherical particles will be produced due to the uniform drying rate of the whole droplet. It can also be observed from the TEM images and HR-TEM images after Cr doping (Fig. 3d and 3e) that there is a significant decrease in the diameter of the catalyst stacked into a spherical shape after Cr doping, and the catalyst generated after doping stacks out smaller particles compared to the undoped catalyst particles. Also, the same lattice stripe spacing (d = 0.40 nm) can be obtained before and after doping, indicating no additional adverse effect on the crystallinity and crystal structure of the catalyst after Cr doping.

To further verify the doping of Cr, the elemental mapping of the catalyst samples after Cr doping was tested. As you can see by Figs. 4f-k, Mo, V, Te, Nb, and Cr are uniformly distributed in the rod structure of the catalysts, further proving that the Cr atoms are incorporated into the $MoVTeNbO_x$ framework.

The average grain size of the catalysts before and after Cr doping obtained from SEM images is shown in Fig. 4. Here you can see from Fig. 4a and b, the cross-sectional diameters of the rod-like structure of the undoped Cr catalyst sample S-0 were mainly concentrated at 234.21 ± 12.16 nm. The average grain lengths were concentrated between 1.096 ± 0.13 μm. In contrast, the average particle size of the doped S-3 samples was significantly reduced, with the cross-sectional diameters concentrating between 134.96 ± 9.34 nm and the particle length sizes between 485.71 ± 25.21 nm (Fig. 4c, d), which is in agreement with the results obtained by TEM. For $MoVTeNbO_x$ composite metal oxides, the smaller the catalyst's crystal size, the significantly improved the catalytic performance[43]. By the appropriate amount of Cr doping, the particle dimension of the catalyst was reduced, which decreased the diameter and particle length of the catalyst rod structure and increased the specific surface area (Table. 1). At the same time, the number of active crystalline surfaces (001 surfaces) per unit volume of the catalyst increased, and more terminal active sites could be exposed.

As evidenced in Fig. 5, the pore volume distribution of N_2 adsorption obtained before and after Cr doping of the catalyst. Combined with Table. 1, it can be found that the specific surface area of the S-3 catalyst is significantly increased compared to the undoped S-0. Since the catalytic reaction occurs on the surface-active sites, a larger specific surface area can provide more active sites and thus increase the catalytic activity. As can be seen in Fig. 5, the pore radius of the doped catalysts is significantly reduced from 5–10 nm to 2–4 nm. The pore size distribution is more uniform, not only due to the increase in the volume of the catalyst cytosol after doping but also may be due to the more compact random stacking of the catalyst nanoparticles. Based on Figs. 2 and 3, it can be seen that the catalyst stacked out the pore structure. It can be seen that Cr doping not only improves the specific surface area of the trigger, reduces the particle dimension of the catalyst, exposes more active sites, and makes contact with the reactants more adequate but also makes the distribution of mesoporous structures produced by the catalyst stacking more concentrated.

The high-resolution XPS spectra of Mo 3d, V $2p_{3/2}$, Te 3d, Nb 3d and Cr 2p on the surface of the S-0 and S-3 samples are shown in Fig. 6. All peaks were calibrated with the C1s accidental peak at 284.6eV. Figure 6a shows the XPS survey spectra of S-0 and S-3. Figure 6a shows the full elemental mapping of the S-0 and S-3 catalysts. From Fig. 6b, it can be seen that the Mo $3d_{5/2}$ and Mo $3d_{3/2}$ binding energy (BE) peaks of S-0 and S-3 are located at 232.7 ± 0.1 eV and 236.3 ± 0.1 eV, which indicates that Mo is composed of Mo^{6+} (232.5 ± 0.2 eV, 238.8 ± 0.2 eV) and Mo^{5+} (233.5, 236.5 eV) [44, 45]. For V, the element V of the S-0 and S-3 samples is exhibited in Fig. 6c with two valence states, V^{4+} (516.3 eV) and V^{5+} (517.2 eV)[46, 47]. It is reported that breaking the C-H bond is the limiting step in the oxidative dehydrogenation of propane and that this step occurs at the active site consisting of V ions on the surface of the M1 phase. Therefore, V^{5+} ions are considered the active site for alkane activation[48, 49]. In Fig. 6c, it can be seen that the proportion of the V^{5+} peak area of the Cr-doped S-3 catalyst samples was significantly increased, implying that the concentration of V^{5+} on the surface of the catalyst increased after Cr was doped into the framework of the $MoVTeNbO_x$ catalysts, which suggests that the doping of Cr was able to induce the conversion of V^{4+} to V^{5+}. Te $3d_{5/2}$ has a binding energy peak (BE) centered at 576.3 eV[50] (Fig. 6d). The critical energy peak (BE) values detected by Nb 3d can be split into two extremes at 207.2 ± 0.4 eV and 209.7 ± 0.3 eV[43], thus indicating that elemental Nb is mainly composed of Nb^{4+} and Nb^{5+} on the surface of the S-0 and S-3 samples (Fig. 6e). In Fig. 6f, the Cr $2p_{3/2}$ and Cr $2p_{1/2}$ binding energy (BE) peaks were located at 576.3 ± 0.1 eV and 586.5 ± 0.1 eV, which indicated that the Cr element was composed of Cr^{2+}. The results showed that various elemental ions were uniformly attached to the catalyst surface.

Fig .6 XPS survey spectra (a), and high-resolution XPS spectra of (b) Mo 3d, (c) V $2p_{3/2}$, (d) Te 3d, (e) Nb 3d, (f) Cr 2p of S-0 and S-3 samples

3.2 Catalytic performance

The catalytic performance of $MoVTeNbCrO_x$ for oxidative dehydrogenation of propane to acrylic acid was tested at a reaction temperature of 340–420°C. What is presently vividly in the bar chart (Fig. 7) is that shows the results of propane conversion and product selectivity of all samples. From the product selectivity plots of S-3 catalyst at different reaction temperatures (Fig. 7a), it can be seen that at 380°C, the oxidative dehydrogenation of propane produced three by-products, namely, acetic acid, CO_2 and CO, in addition to acrylic acid, among which the highest selectivity to AA was obtained. You can see from the Fig. 7b, at 380°C, selectivity to AA tended to increase first and then decrease with the increase of doping ratio. Compared to the S-0 sample of $MoVTeNbO_x$, the S-3 sample showed the highest selectivity against AA among all catalysts at 84.3%, with a high propane conversion at 47.6%. The catalytic performance of the other samples was poor, in which the selectivity to AA of the S-1, S-2, and S-5 catalyst samples was lower than that of the undoped $MoVTeNbO_x$ (S-0), in which the selectivity to AA of S-5 was only 53.04%, and the propane conversion was 35.6%. This suggests that too much or too little doping affects the catalyst performance. The poor performance due to too low doping may be because there are not enough Cr atoms to make up for the atomic vacancies left by the loss of Te, resulting in the absence of the M1

phase structure and the reduction of the number of active sites. Excessive doping leads to the covering of active sites on the catalyst surface, which may also be the reason for the decrease selectivity to AA. At the doping amount of V: Cr = 1:0.015, the catalyst activity was the highest, which was conducive to promoting AA generation and propane conversion.

Also, the suitable Mesoporous structure facilitates the diffusion and transport of reactants and products, prevents deep oxidation, and improves. Cr doping has resulted in a substantial increase in the specific surface area of the catalyst and a more concentrated pore size distribution. At the same time, the Mesoporous structure generated by the random stacking of catalysts fully exposes the active sites, leading to an increase in the number of active sites in contact with the feedstock, and the appropriate temperature is more favorable for improving catalytic performance. The results show that Cr doping dramatically improves the performance of $MoVTeNbO_x$ catalysts, but excessive Cr doping negatively affects the catalytic performance.

S-3 catalyst at 340–420°C (a), (b) Conversion and product selectivity of $MoVTeNbCrO_x$ samples at 380°C

The conversion of all samples increases with increasing temperature at 340–420°C (Fig. 8). Except for sample S-5, the propane conversion of all models was higher than that of $MoVTeNbO_x$ (S-0), with the highest conversion of sample S-1, which was 59.3% at 420°C. With the introduction of Cr, the transformation of propane decreased. In this work, the catalyst stability study was carried out under reaction conditions: temperature 380°C, catalyst dosage 0.75 g, feed gas ratio C_3H_8: O_2: N_2: H_2O = 1.0: 6.2: 4.0: 2.0, propane flow rate 2 $mL.min^{-1}$. The stability of the catalyst was investigated, and the results showed that the selectivity of the catalyst to acrylic acid, the yield to acrylic acid, and the conversion of propane were consistently maintained 55.2%,79.5% and 43.2% within 80 h, and chromium doping did not affect the stabilizing effect of the catalyst. (Fig. 9).

4. Conclusions

We investigated the crystal structure and the catalytic performance of pure M1 pophase $MoVTeNbO_x$ and Cr-doped $MoVTeNbCrO_x$ prepared by spray-drying method for the direct oxidation of propane to acrylic acid. The results showed that the catalysts' cell volume, particle size, and surface V^{5+} content could be changed by varying the molar ratio of V: Cr. TEM, XPS, and cell parameter calculation studies confirmed the elemental insertion into the M1 phase structure. Catalyst particles of rod stacked spherical shape were prepared by doping Cr. The cross-sectional diameters of the M1 phase particles ranged from 134.96 ± 9.34 nm, and the particle length dimensions were 485.71 ± 25.21 nm. The spherical particles were also smoother and more regular than the undoped samples. Not only that, by doping, the mesopore structure formed by randomly stacking the catalysts into spheres becomes more concentrated, and the pore radius is uniformly distributed in the range of 2–4 nm.

The surface V^{5+} content reached 72.6% at V: Cr = 1:0.015. In addition, the prepared $MoVTeNbCrO_x$(S-3) catalyst exhibited excellent catalytic performance for the selective oxidation of propane at 380°C. The

conversion of propane and the selectivity of AA were 55.2% and 79.5%, respectively, and the yield of AA could reach 43.2%.

Declarations

Conflict of interest:
On behalf of editor, the corresponding author states that there is no conflict of interest.

Author Contribution

HN Q wrote the main manuscript textSM L,YW W,J S,Z L,SS Y,YT Z,RQ Z responsible for reviewingAll authors reviewed the manuscript

Acknowledgements

The authors gratefully acknowledge the financial supports by the National Natural Science Foundation of China (No. 21706165), LiaoNing Revitalization Talents Program (No. XLYC2002001), Shenyang Young and Middle-aged Science and Technology Innovation Talent Support Program, China (No. RC210184) and Applied Basic Research Programs of Liaoning Province (No. 2023JH2/101300243). Basic Research Projects of Liaoning Provincial Department of Education, China (No. JYTMS20231497)

References

1. Gao D, Zhang Y, Lyu B, Wang P, Ma J(2019)Nanocomposite based on poly acrylic acid attapulgite towards flame retardant of cotton fabrics. Carbohydr Pol 206: 245–253.http://10.1016/j.carbpol.2018.10.113
2. Saurabh.Vijay OPS, Dipak K Majumdar(2011)Acrylic acid-methyl methacrylate (2.57.528) enteric copolymer for colon targeted drug delivery. J Mater Sci Mater Med 22(1): 125–135http://10.1007/s10856-010-4192-4
3. Kardash TY, Lazareva EV, Svintsitskiy DA, Kovalev EP, Bondareva VM (2019)Effect of Selenium Additives on the Physicochemical and Catalytic Properties of MoVTeNbO Catalysts in the Oxidative Dehydrogenation of Ethane. KiCat60(3): 355–365http://10.1134/s0023158419030078
4. Chen Y, Yan B, Cheng Y(2023)Microporous exposure on catalytic performance of $MoVNbTeO_x$ mixed metal oxides in the oxidative dehydrogenation of ethane. JCat426: 308 –18.http://10.1016/j.jcat.2023.07.025
5. Jung-Hyun Park C-, H S((2015) Oxidative dehydrogenation of butenes to butadiene over Bi–Fe–Me(Me = Ni, Co, Zn, Mn and Cu)–Mo oxide catalysts. J Ind Eng Chem 21:683–688.

.http://10.1016/j.jiec.2014.03.037

6. Li S, Lu Z, Yan Y, Deng L, Fan Y, Zhu N, Xu L, Yu S (2021)The Structure and Catalytic Properties of $MoVTeNbO_x$ Catalysts Modified by Adding Cr, Fe, Ce and W. Catal Surv Asia26(1): 58–67http://10.1007/s10563-021-09346-4
7. Zenkovets GA, Bondareva VM, Shutilov AA, Sobolev VI, Marchuk AS, Tsybulya SV, Prosvirin IP, Suprun EA, Ishchenko AV, Gavrilov V Y(2022)Multicomponent $MoVSbNbGdO_x/SiO_2$ catalyst in oxidative dehydrogenation of ethane: Effect of Gd on catalytic properties. Appl Catal A-Gen633.http://10.1016/j.apcata.2022.118536
8. Dang D, Chen Y, Chen X, Feng K, Yan B, Cheng Y(2022)Phase-pure M1 $MoVNbTeO_x/TiO_2$ nanocomposite catalysts: high catalytic performance for oxidative dehydrogenation of ethane. Catal Sci Technol 12(4): 8.http://10.1039/d1cy01749g
9. Concepción S P, H JM, López Nieto(2011)On the nature of active sites in MoVTeO and MoVTeNbO catalysts: The influence of catalyst activation temperature. Appl Catal A- Gen391(1–2): 92–101.http://10.1016/j.apcata.2010.05.011
10. Hernández-Morejudo S, Massó A, García-González E, Concepción P, López Nieto JM (2015) Preparation, characterization and catalytic behavior for propane partial oxidation of Ga-promoted MoVTeO catalysts. Appl Catal A- Gen504:51–61. http://10.1016/j.apcata.2014.12.039
11. Ishchenko EV, Gulyaev RV, Kardash TY, Ishchenko AV, Gerasimov EY, Sobolev VI, Bondareva VM (2017)Effect of Bi on catalytic performance and stability of MoVTeNbO catalysts in oxidative dehydrogenation of ethane. Appl Catal A- Gen534: 58–69.http://10.1016/j.apcata.2017.01.023
12. Deniau B, Millet JMM, Loridant S, Christin N, Dubois JL (2008) Effect of several cationic substitutions in the M1 active phase of the MoVTeNbO catalysts used for the oxidation of propane to acrylic acid. JCat260(1): 30–36http://10.1016/j.jcat.2008.08.020
13. Lazareva EV, Bondareva VM, Svintsitskii DA, Kardash TY (2020)Preparing MoVTeNbBiO Catalysts for the Selective Oxidative Conversion of Light Alkanes. Catal Ind 12(1): 39–46.http://10.1134/s2070050420010092
14. Yun YS, Lee M, Sung J, Yun D, Kim TY, Park H, Lee KR, Song CK, Kim Y, Lee J, Seo Y-J, Song IK, Yi J(2018)Promoting effect of cerium on MoVTeNb mixed oxide catalyst for oxidative dehydrogenation of ethane to ethylene. Appl Catal B-Environ237: 554 – 62.http://10.1016/j.apcatb.2018.06.025
15. Chen Y, Qian S, Feng K, Wang Y, Yan B, Cheng Y(2022)$MoVNbTeO_x$ M1@CeO_2@Cordierite structured catalysts for ODHE process. ChEnS253.http://10.1016/j.ces.2022.117597
16. Yan P, Chen Y, Cheng Y (2022)Industrially potential $MoVNbTeO_x$@FoamSiC structured catalyst for oxidative dehydrogenation of ethane. Chem Eng J427 http://10.1016/j.cej.2021.131813
17. Chu B, An H, Chen X, Cheng Y (2016)Phase-pure M1 $MoVNbTeO_x$ catalysts with tunable particle size for oxidative dehydrogenation of ethane. Appl Catal A- Gen524: 56–65.http://10.1016/j.apcata.2016.05.026

18. Chen X, Dang D, An H, Chu B, Cheng Y (2019))MnO_x promoted phase-pure M1 MoVNbTe oxide for ethane oxidative dehydrogenation. J Taiwan Inst Chem E95:103–111. http://10.1016/j.jtice.2018.10.004
19. Tu X, Niwa M, Arano A, Kimata Y, Okazaki E, Nomura S(2018)Controlled silylation of MoVTeNb mixed oxide catalyst for the selective oxidation of propane to acrylic acid. Appl Catal A-Gen 549: 152–160.http://10.1016/j.apcata.2017.09.013
20. Valente JS, Maya-Flores E, Armendáriz-Herrera H, Quintana-Solórzano R, López Nieto J M(2018)Metal solution precursors: their role during the synthesis of MoVTeNb mixed oxide catalysts. Catal Sci Technol 8(12): 3123–3132.http://10.1039/c8cy00750k
21. Li M, Huang X, Zhang G, Tang Z, Hu D(2023)Elaborating the improving SO_2 resistance mechanism of CeWTi catalysts through framework confined ordered mesoporous structures for low-temperature NH_3-SCR reaction. Sep Purif Technol324 http://10.1016/j.seppur.2023.124555
22. Kolen'ko YV, Zhang W, d'Alnoncourt RN, Girgsdies F, Hansen TW, Wolfram T, Schlögl R Trunschke A(2011)Synthesis of MoVTeNb Oxide Catalysts with Tunable Particle Dimensions. ChemCatChem3(10): 1597–1606http://10.1002/cctc.201100089
23. Troyano J, Çamur C, Garzón-Tovar L, Carné-Sánchez A, Imaz I Maspoch D(2020)Spray-Drying Synthesis of MOFs, COFs, and Related Composites. Acc Chem Res 53(6): 1206–1217.http://10.1021/acs.accounts.0c00133
24. Zhu G, Li Q, Zhao Y, Che R (2017) Nanoporous $TiNb_2O_7$/C Composite Microspheres with Three-Dimensional Conductive Network for Long-Cycle-Life and High-Rate-Capability Anode Materials for Lithium-Ion Batteries. ACS Appl Mater Interfaces 9(47):41258–41264. http://10.1021/acsami.7b13246
25. Malamatari M, Charisi A, Malamataris S, Kachrimanis K, Nikolakakis I(2020)Spray Drying for the Preparation of Nanoparticle-Based Drug Formulations as Dry Powders for Inhalation. Processes8(7).http://10.3390/pr8070788
26. Li X, Zhang M, You W, Pei K, Zeng Q, Han Q, Li Y, Cao H, Liu X, Che R (2020)Magnetized MXene Microspheres with Multiscale Magnetic Coupling and Enhanced Polarized Interfaces for Distinct Microwave Absorption via a Spray-Drying Method. ACS Appl Mater Interfaces 12(15): 18138–18147.http://10.1021/acsami.0c00935
27. Ishchenko EV, Popova GY, Kardash TY, Ishchenko AV, Plyasova LM, Andrushkevich T V(2013)Role of MoVTeNb oxide catalyst constituent phases in propane oxidation to acrylic acid. Catal Sustainable Energy1 http://10.2478/cse-2013-0003
28. Baca M, Aouine M, Dubois J, Millet J(2005)Synergetic effect between phases in MoVTe(Sb)NbO catalysts used for the oxidation of propane into acrylic acid. JCat233(1): 234–241http://10.1016/j.jcat.2004.12.002
29. Chen Y, Dang D, Yan B, Cheng Y(2022)Nanocomposite catalysts of non-purified $MoVNbTeO_x$ with CeO_2 or TiO_2 for oxidative dehydrogenation of ethane. ChEnS264.http://10.1016/j.ces.2022.118154

30. Hävecker M, Wrabetz S, Kröhnert J, Csepei L-I, Naumann d'Alnoncourt R, Kolen'ko YV, Girgsdies F, Schlögl R Trunschke A(2012)Surface chemistry of phase-pure M1 MoVTeNb oxide during operation in selective oxidation of propane to acrylic acid. JCat285(1): 48–60http://10.1016/j.jcat.2011.09.012
31. Qian S, Chen Y, Yan B, Cheng Y(2022)Plasma treated M1 $MoVNbTeO_x$–CeO_2 composite catalyst for improved performance of oxidative dehydrogenation of ethane. Green Energy Environ http://10.1016/j.gee.2022.01.001
32. Han Z, Tang C, Sha F, Tang S, Wang J, Li C (2021))CO_2 hydrogenation to methanol on ZnO-ZrO_2 solid solution catalysts with ordered mesoporous structure. JCat396: 242 – 50.http://10.1016/j.jcat.2021.02.024
33. Yang Q, Wang H, Li F, Dang Z, Zhang L(2021)Rapid and efficient removal of Cr( ) by a core–shell magnetic mesoporous polydopamine nanocomposite: roles of the mesoporous structure and redox-active functional groups. J Mater Chem A9(22): 13306–13319.http://10.1039/d1ta02475b
34. Lapisardi G, Chiker F, Launay F, Nogier J-P, Bonardet J-L (2004)A one-pot synthesis of adipic acid from cyclohexene under mild conditions with new bifunctional Ti-AlSBA mesostructured catalysts. Catal Commun 5(6): 277–281http://10.1016/j.catcom.2004.03.005
35. Ishchenko EV, Kardash TY, Gulyaev RV, Ishchenko AV, Sobolev VI, Bondareva VM (2016) Effect of K and Bi doping on the M1 phase in MoVTeNbO catalysts for ethane oxidative conversion to ethylene. Appl Catal A- Gen514:1–13. http://10.1016/j.apcata.2015.12.018
36. Li H, Ban L, Wang Z, Meng P, Zhang Y, Wu R, Zhao Y(2019)Regulation of Cu Species in CuO/SiO_2 and Its Structural Evolution in Ethynylation Reaction. Nanomaterials9(6).http://10.3390/nano9060842
37. Grasselli RK, Buttrey DJ, DeSanto P, Burrington JD, Lugmair CG, Volpe AF, Weingand T(2004)Active centers in Mo–V–Nb–Te–O_x (amm)oxidation catalysts. Catal Today 91-92: 251–258.http://10.1016/j.cattod.2004.03.060
38. Ramírez M, d l Á, Bindini E, Moretti P, Soler Illia GJAA, Amenitsch H, Andreozzi P, Ortore MG, Moya S E(2022)Impact of PEGylation on the degradation and pore organization in mesoporous silica nanoparticles: A study of the inner mesoporous structure in physiologically relevant ionic conditions. Colloid Surf B219 http://10.1016/j.colsurfb.2022.112797
39. Wu Z-Y, Zhu P, Cullen DA, Hu Y, Yan Q-Q, Shen S-C, Chen F-Y, Yu H, Shakouri M, Arregui-Mena JD, Ziabari A, Paterson AR, Liang H-W Wang H(2022)A general synthesis of single atom catalysts with controllable atomic and mesoporous structures. Nat Synthesis 1(8): 658–667http://10.1038/s44160-022-00129-x
40. Wang Y, Fan Y, Li S, Wang Y, Chen Y, Liu D, Wei W, Yu S (2022) Crystal structure and catalytic performance for direst oxidation of propylene to acrylic acid of $MoVTeNbO_x$ prepared by high-pressure hydrothermal synthesis. RCM1(3–4): 211 – 21.http://10.1016/j.recm.2022.07.004
41. Fan Y, Li S, Liu Y, Wang Y, Wang Y, Chen Y, Yu S (2022) High-pressure hydrothermal synthesis of $MoVTeNbO_x$ with high surface V^{5+} abundance for oxidative conversion of propane to acrylic acid. J Supercrit Fluid181. http://10.1016/j.supflu.2021.105469

42. Boel E, Koekoekx R, Dedroog S, Babkin I, Vetrano MR, Clasen C Van den Mooter G(2020)Unraveling Particle Formation: From Single Droplet Drying to Spray Drying and Electrospraying. Pharmaceutics12(7).http://10.3390/pharmaceutics12070625
43. Ramírez-Salgado J, Quintana-Solórzano R, Mejía-Centeno I, Armendáriz-Herrera H, Rodríguez-Hernández A, Guzmán-Castillo Md, L, Valente J S(2022)On the role of oxidation states in the electronic structure via the formation of oxygen vacancies of a doped $MoVTeNbO_x$ in propylene oxidation. ApSS573.http://10.1016/j.apsusc.2021.151428
44. Svintsitskiy DA, Kardash TY, Lazareva EV, Bondareva V M(2021)X-ray-induced transformations on the surface of MoVNbTe mixed oxide catalyst: An XPS study. ApSS535.http://10.1016/j.apsusc.2020.147676
45. Svintsitskiy DA, Kardash TY, Lazareva EV, Saraev AA, Derevyannikova EA, Vorokhta M, Šmíd B, Bondareva V M(2019)NAP-XPS and in situ XRD study of the stability of Bi-modified MoVNbTeO catalysts for oxidative dehydrogenation of ethane. Appl Catal A-Gen579: 141 – 50 http://10.1016/j.apcata.2019.04.027
46. Li S, Liu Y, Fan Y, Lu Z, Yan Y, Deng L, Zhang Z, Yu S (2020) Facile sub-/supercritical water synthesis of nanoflake $MoVTeNbO_x$-mixed metal oxides without post-heat treatment and their catalytic performance. RSC Adv 10(65):39922–39930. http://10.1039/d0ra06877b
47. Annamalai L, Ezenwa S, Dang Y, Tan H, Suib SL, Deshlahra P(2021)Comparison of structural and catalytic properties of monometallic Mo and V oxides and M1 phase mixed oxides for oxidative dehydrogenation. Catal Today 368: 28–45.http://10.1016/j.cattod.2020.04.046
48. Tompos A, Sanchez-Sanchez M, Végvári L, Szijjártó GP, Margitfalvi JL, Trunschke A, Schlögl R, Wanninger K Mestl G(2021)Combinatorial optimization and synthesis of multiple promoted MoVNbTe catalysts for oxidation of propane to acrylic acid. Catal Today 363: 45–54.http://10.1016/j.cattod.2019.03.047
49. Quintana-Solorzano R, Mejia-Centeno I, Armendariz-Herrera H, Ramirez-Salgado J, Rodriguez-Hernandez A, Guzman-Castillo ML, Lopez Nieto JM, Valente JS (2021)Discerning the Metal Doping Effect on Surface Redox and Acidic Properties in a $MoVTeNbO_x$ for Propa(e)ne Oxidation. ACS Omega 6(23): 15279–15291.http://10.1021/acsomega.1c01591
50. Chen Y, Dang D, Yan B, Cheng Y (2022)Mixed Metal Oxides of M1 $MoVNbTeO_x$ and TiO_2 as Composite Catalyst for Oxidative Dehydrogenation of Ethane. Catalysts12(1).http://10.3390/catal12010071

Figures

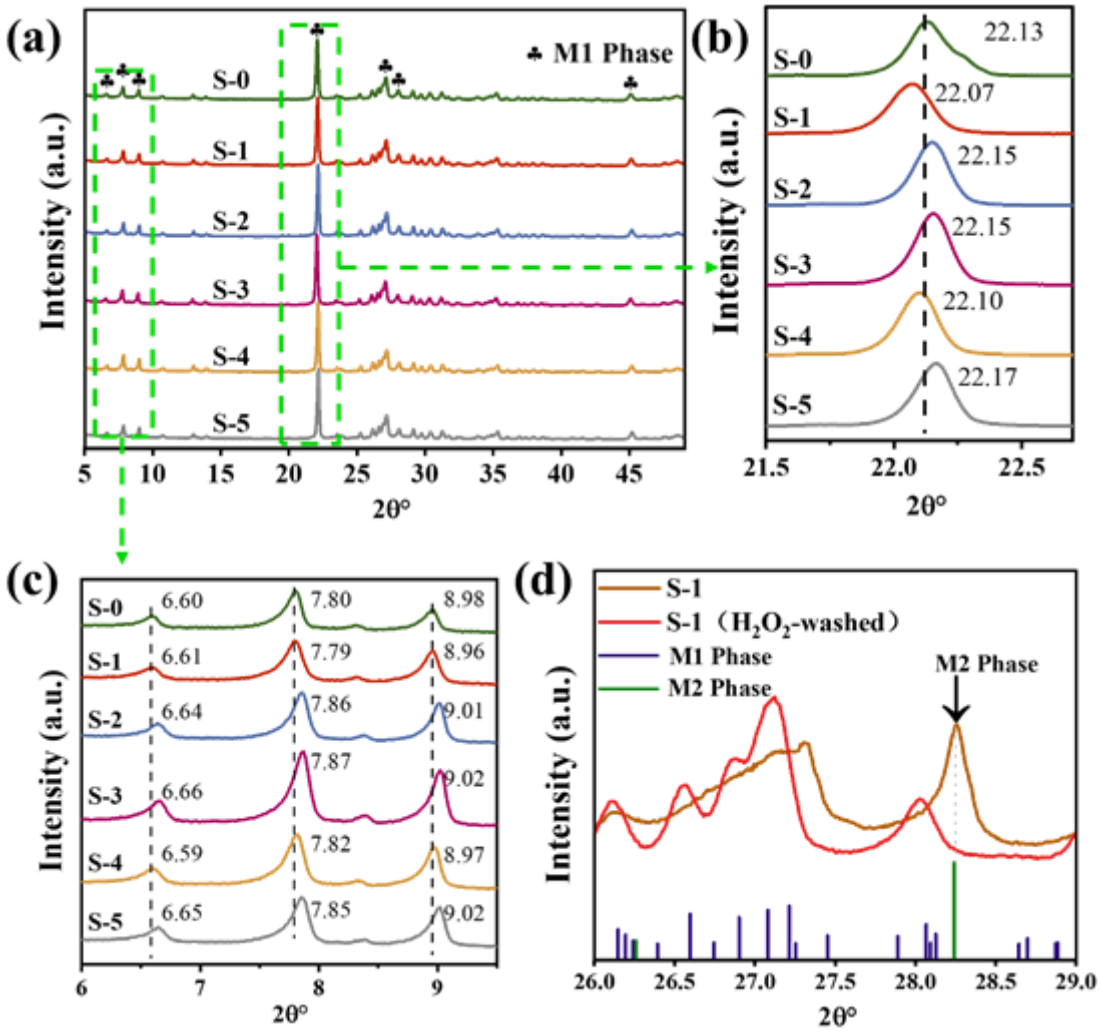

Figure 1

(a) XRD patterns of $MoVTeNbO_x$ and $MoVTeNbCrO_x$ doped with different proportions of $MoVTeNbCrO_x$, (b) and (c) are the detailed patterns of the zone marked with dotted lines in Fig. a, respectively,(d) XRD patterns of the catalysts before and after the post-treatment by H_2O_2 at 26-29 °

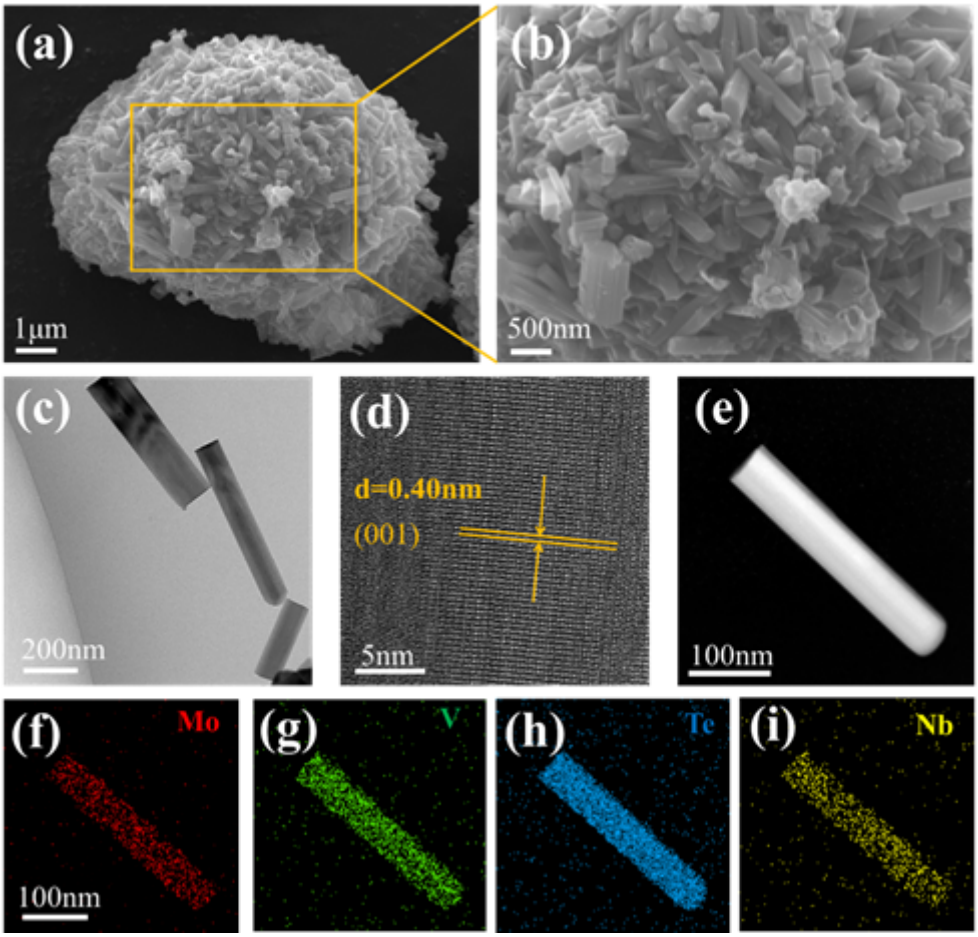

Figure 2

(a) and (b) are scans SEM images of S-0 at different multiples, (c) TEM, (d) HR-TEM, and (e-i) elemental mapping images of S-0

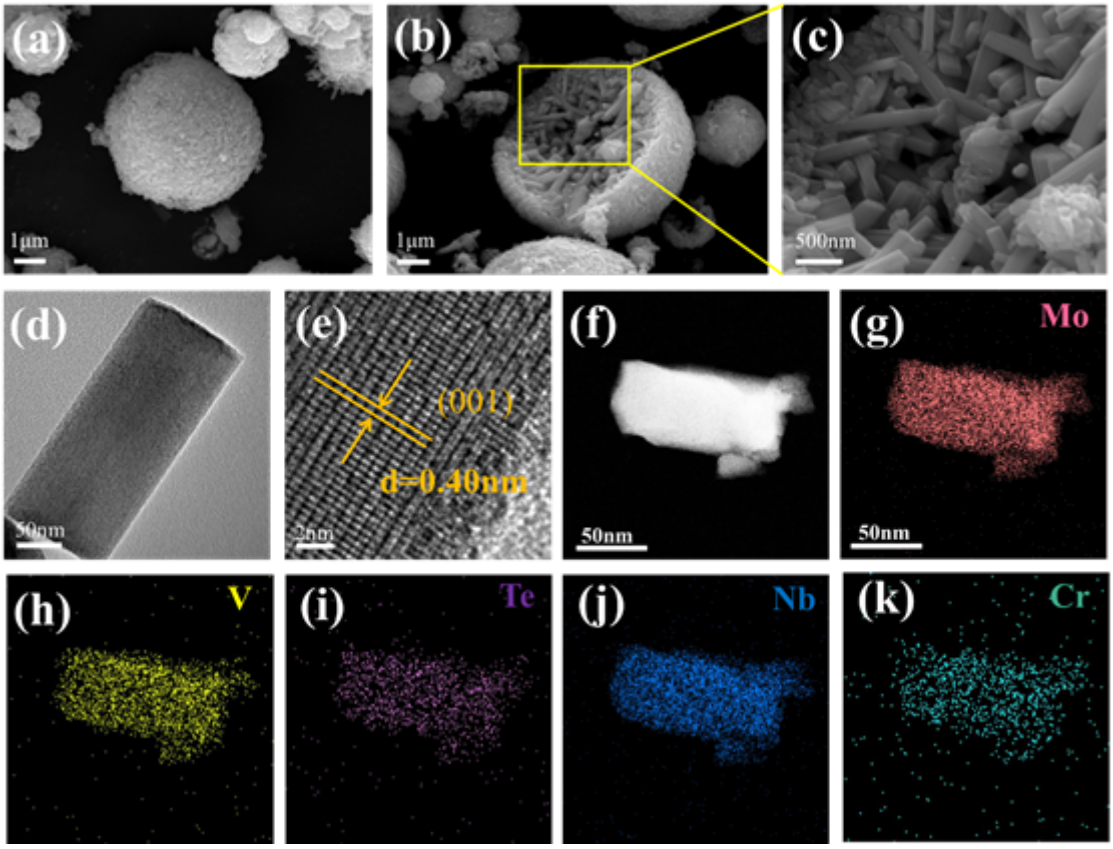

Figure 3

(a) and (b) are the scans SEM images of S-3 at different positions, (c) is the amplified spectrum of (b), (d) TEM, (e) HR-TEM, and (f-k) elemental mapping images of S-3

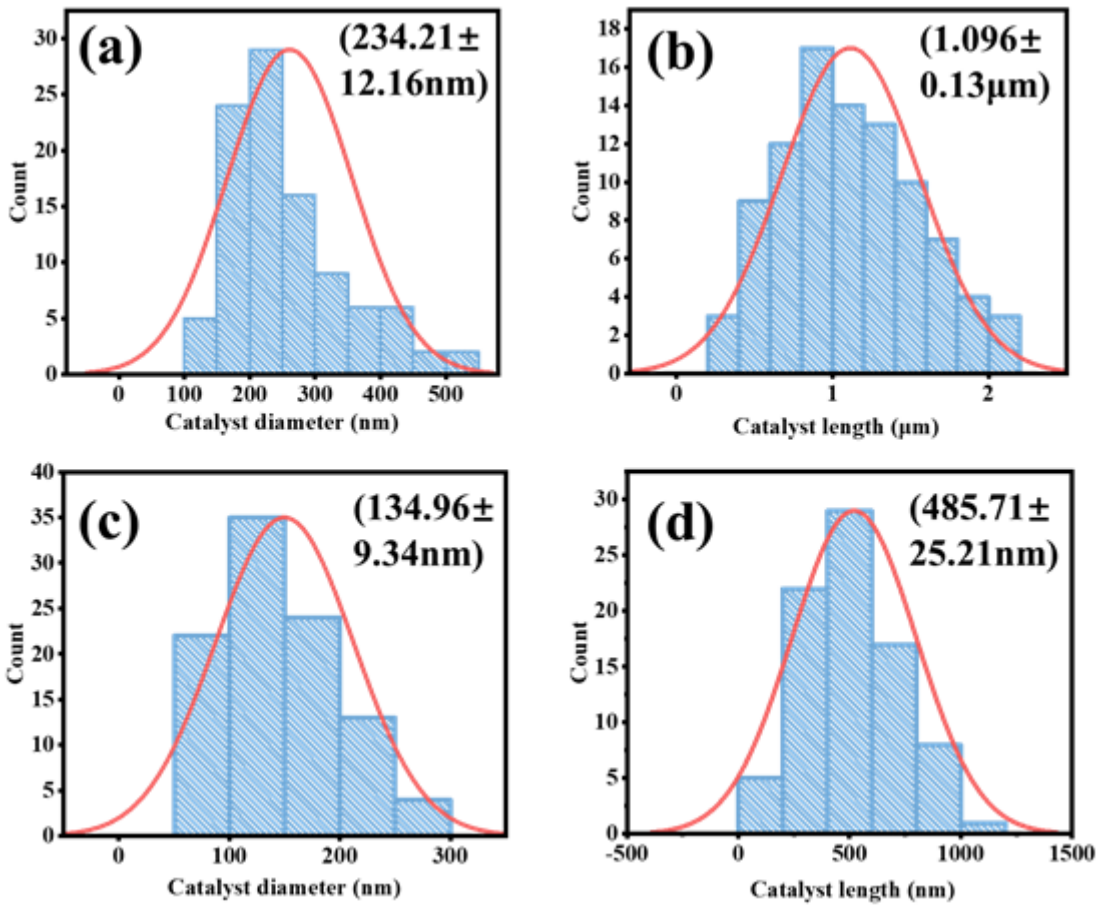

Figure 4

Plots of average particle size dimensions of catalysts before and after Cr doping, (a) bar cross-section diameter of S-0, (b) bar particle length of S-0, (c) S-3 bar cross-section diameter of S-3, (d) bar particle length of S-3

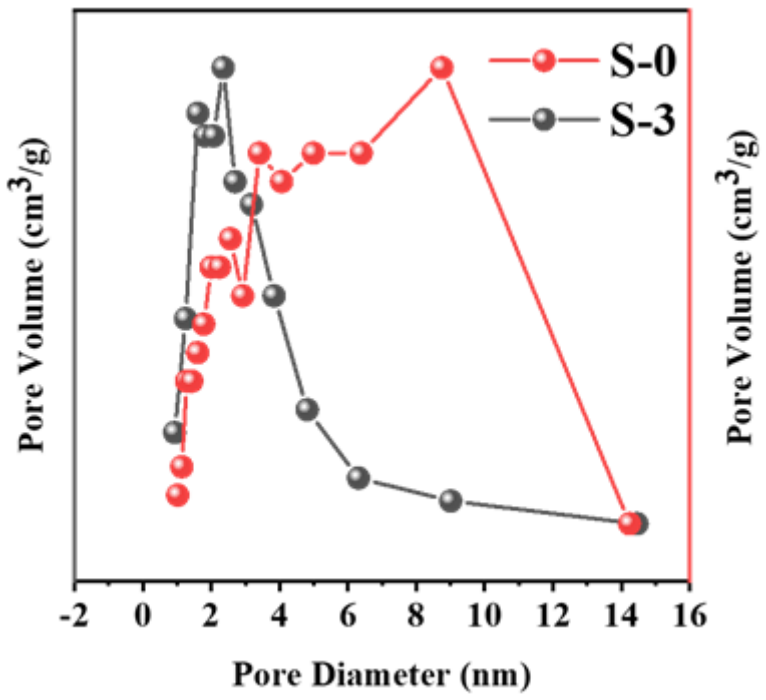

Figure 5

Adsorption pore volume distribution curves of S-0 and S-3

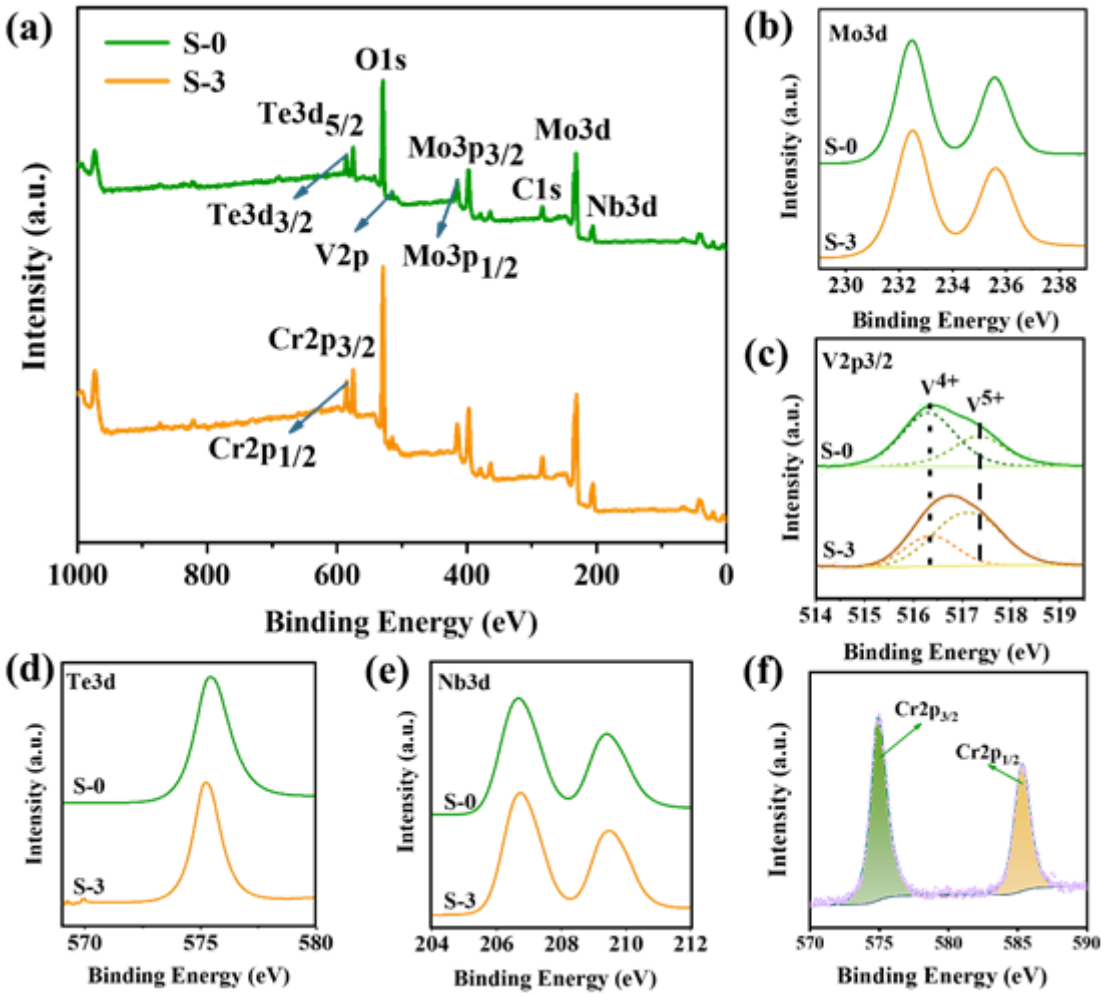

Figure 6

XPS survey spectra (a), and high-resolution XPS spectra of (b) Mo 3d, (c) V $2p_{3/2}$, (d) Te 3d, (e) Nb 3d, (f) Cr 2p of S-0 and S-3 samples

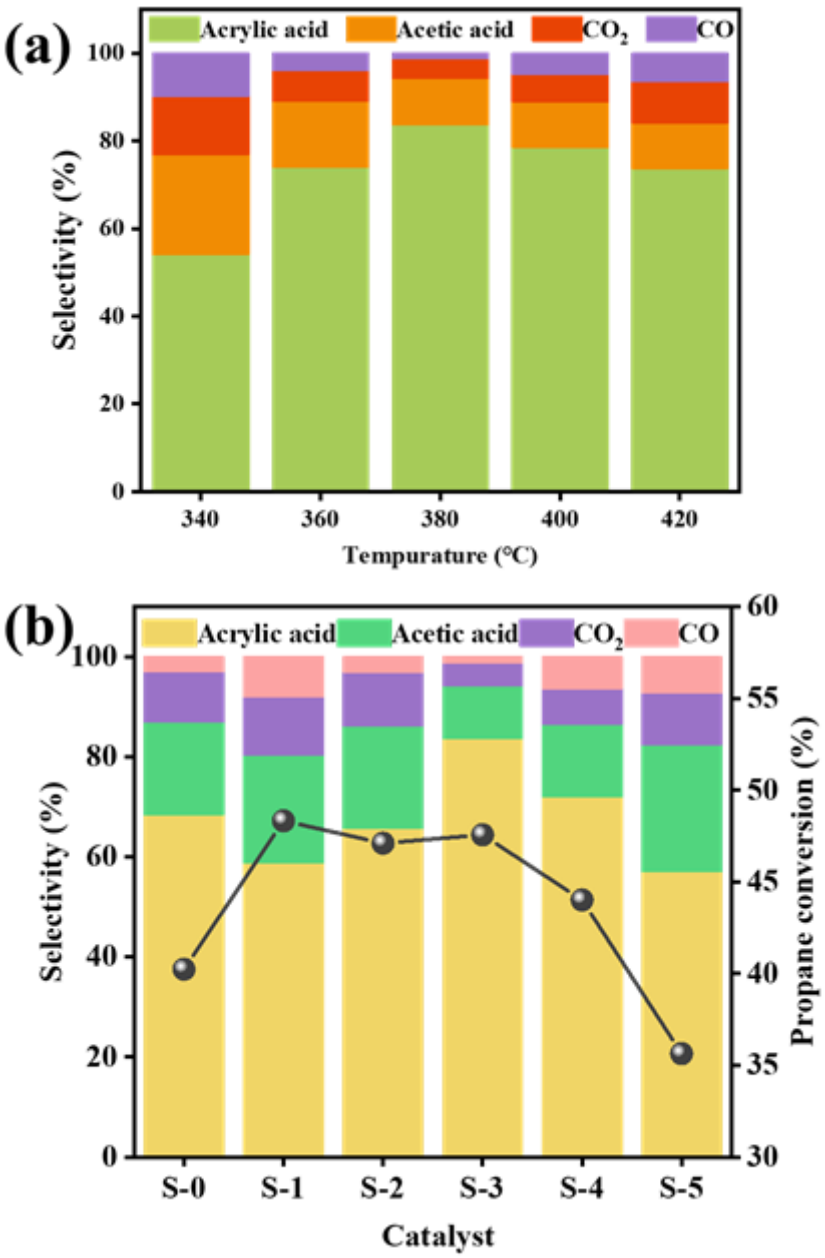

Figure 7

Selectivities to reaction product of propane oxidation catalyzed by

S-3 catalyst at 340-420 °C (a), (b) Conversion and product selectivity of $MoVTeNbCrO_x$ samples at 380 °C

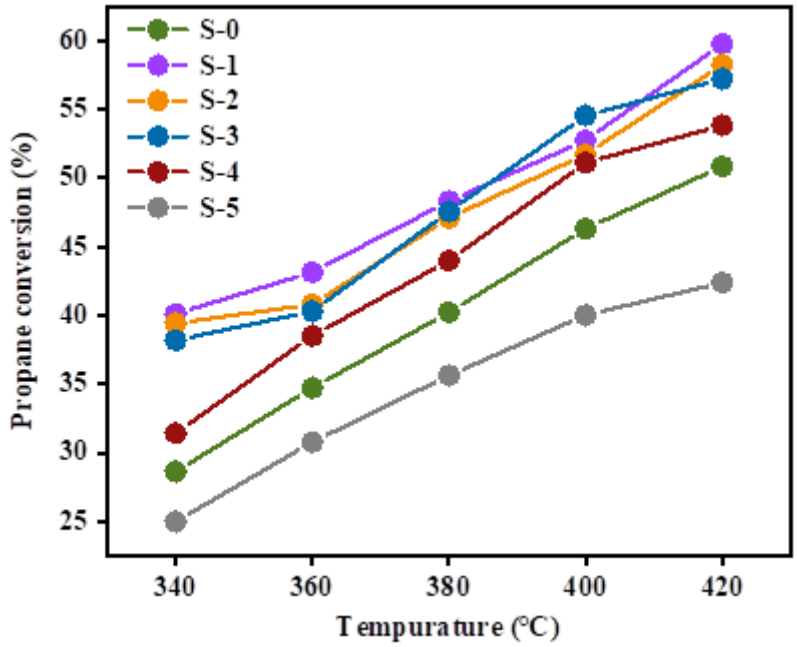

Figure 8

Conversion of all samples at different reaction temperatures

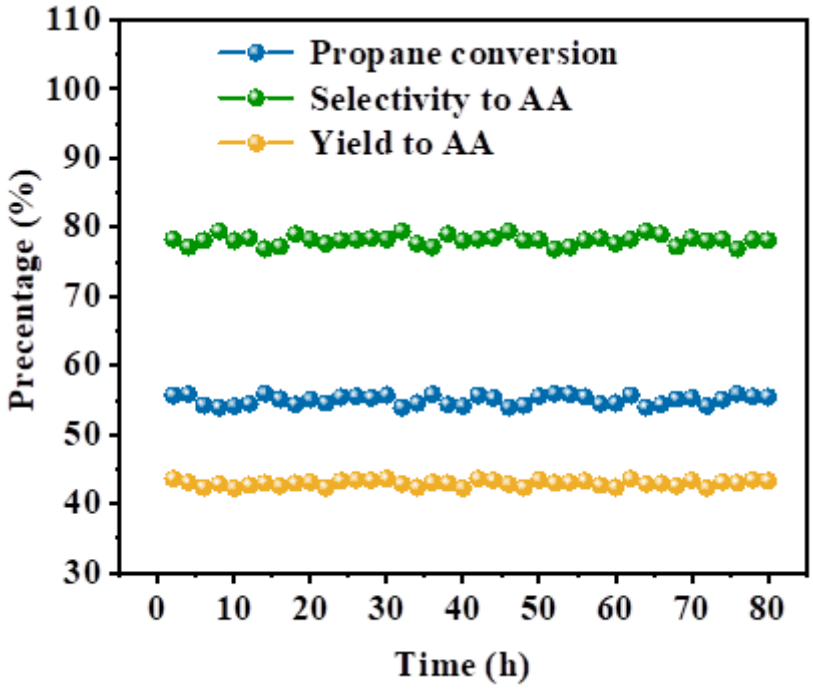

Figure 9

Stability test of $MoVTeNbCrO_x$ (S-3) catalyst over 80 h. Reaction conditions: temperature 380 **°C**, catalyst dosage 0.75 g, feed gas ratio C_3H_8: O_2: N_2: H_2O = 1.0: 6.2: 4.0: 2.0 propane flow rate 2 $mL.min^{-1}$